



Bi₂(Sn_{0.95}Cr_{0.05})₂O₇: Structure, IR spectra, and dielectric properties

S.S. Aplesnin^{a,b}, L.V. Udob^{a,*}, M.N. Sitnikov^b, N.P. Shestakov^a

^aKirensky Institute of Physics, Russian Academy of Sciences, Siberian Branch, Akademgorodok 50, bld. 38, Krasnoyarsk, 660036 Russia

^bSiberian State Aerospace University, Krasnoyarsk 660014, Russia

Received 27 October 2015; received in revised form 23 November 2015; accepted 9 December 2015

Available online 18 December 2015

Abstract

Infrared absorption spectra of the bismuth pyrostannate Bi₂(Sn_{0.95}Cr_{0.05})₂O₇ were investigated in the frequency range 350–1100 cm^{−1} at temperatures of 110–525 K. Four frequency regions with split absorption lines are distinguished. Softening of frequencies at the structural transitions was observed. The maxima of permittivity measured in the frequency range 1–200 kHz at temperatures 100–400 K were determined. It was found that the magnetic susceptibility changes its sign in the low-temperature region. The correlation between anomalies in the magnetic susceptibility, permittivity, and absorption line intensity was established. Softening of frequencies is explained by the variation in the coefficient of thermal expansion of the lattice. The temperature behavior of permittivity is described using the Debye model.

© 2015 Elsevier Ltd and Techna Group S.r.l. All rights reserved.

Keywords: Bismuth pyrostannate; Infrared absorption spectra; Structural transition; Permittivity; Debye model

1. Introduction

In recent years, ternary metal oxides with the pyrochlore structure and general chemical formula A₂B₂X₇, where A is the cation (Ca, K, Ce, or Bi), B is the metal cation (Nb, Ta, Ti, or Sn), and X is the anion (O^{2−}, OH[−], or F[−]), have been intensively investigated [1]. These compounds exhibit diverse physicochemical properties. In particular, A₂Ti₂O₇ behaves like spin ice when A is Dy or Ho [2–4], like spin liquid when A is Tb [5,6], and is characterized by antiferromagnetic ordering at low temperatures when A is Er or Gd [7–9]. The Gd₂Ti₂O₇ and Y₂Ti₂O₇ compounds demonstrate high ionic conductivity upon partial substitution of Zr⁴⁺ for Ti⁴⁺, while Gd₂Re₂O₇ is a superconductor [10].

The variety of physical characteristics of the pyrochlore compounds makes it possible to use them as electrolytes for fuel cells and gas sensors [11,12]. The bismuth pyrostannate Bi₂Sn₂O₇ attracts attention of researchers as a catalyst, which can be used, e.g., in oxidation of hydrocarbonates [13] and

isobutene [14–16], as well as an active element for gas sensors [17–19].

The Bi₂Sn₂O₇ crystal structure undergoes a number of polymorphic transitions: below 90 °C, the α-phase and intermediate cubic structure without symmetry center (β-фаза) are observed [20]. The authors of [20, 21] observed the α→β transition at 135 °C and the second harmonic generation with domains on polycrystalline samples. Based on these results, it was assumed that the α-phase and α→β transition are ferroelectric. Neutron diffraction study of the bismuth pyrostannate showed that at 626 °C the β→γ transition occurs, which is related to the displacement of Bi³⁺ ions. According to the X-ray and neutron diffraction data, the α-phase is stable below 137 °C and belongs to the space group *Pc(C₃²)*. The crystal structure of the α-phase is complex and contains 176 atoms. At the temperature of the first phase transition, the unit cell is distorted [22]. The β-phase structure determined by neutron and synchrotron X-ray diffraction is cubic with sp. gr. *F43c(T_d⁵)* [23]. Further synchrotron investigations [24] showed that the β-phase belongs to the trigonal structure with sp. gr. *P3₁(C₃²)*. The cubic and tetragonal phases are similar and can be attributed to the cubic pyrochlore structure.

*Corresponding author. Tel.: +7 391 243 26 35; fax: +7 391 243 89 23.

E-mail address: luba@iph.krasn.ru (L.V. Udob).

As is known, synthesis conditions affect the crystal structure of synthesized compounds. Using the solid-state synthesis, two $\text{Bi}_2\text{Sn}_2\text{O}_7$ polymorphic modifications, orthorhombic and cubic, coexisting at room temperature, were obtained [25]. The $\text{Bi}_2(\text{Sn}_{x}\text{Cr}_{1-x})_2\text{O}_7$ compounds were synthesized by substitution of 3d metals for cations [26,27].

Scanning calorimetry investigations of the $\text{Bi}_2(\text{Sn}_x\text{Cr}_{1-x})_2\text{O}_7$ solid solutions [28] showed two new structural transitions at temperatures of 473 and 646 K, which are atypical for the bismuth stannate $\text{Bi}_2\text{Sn}_2\text{O}_7$, where the $\alpha \rightarrow \beta$ structural transition occurs at $T=370$ K and the transition from the orthorhombic to cubic phase, at $T=548$ K. The presence of two more endothermic peaks is apparently related to local strains of the orthorhombic and cubic structures, which are accompanied by the occurrence of maxima in the temperature dependence of resistivity due to rearrangement of the electronic structure.

The mechanisms of the observed structural transitions can be elucidated by infrared (IR) spectroscopy. The types of bonds and cations, whose displacements lead to the lattice strain, can be determined by monitoring the variation in the frequency of oscillations of certain modes. The aim of this study was to investigate the effect of substitution of chromium ions in the $\text{Bi}_2(\text{Sn}_{0.95}\text{Cr}_{0.05})_2\text{O}_7$ on its dynamic properties in the IR spectral range and to establish the correlation between the structural variations and dielectric properties of the compound.

2. Experimental

The $\text{Bi}_2(\text{Sn}_{0.95}\text{Cr}_{0.05})_2\text{O}_7$ samples were synthesized using the solid-state reaction technique described in detail in [25]. According to the X-ray data, the synthesized compound exists simultaneously in the cubic and orthorhombic polymorphic modifications. As in the $\text{Bi}_2\text{Sn}_2\text{O}_7$ compound [25,29], the

fraction of cubic phase is larger than that of orthorhombic one. The parameters of the cubic phase (sp. gr. Fd3m) are $a=10.69\text{ \AA}$ and $V=222.42(9)\text{ \AA}^3$ and the parameters of the orthorhombic phase (sp. gr. Pmmm) are $a=3.782\text{ \AA}$, $b=7.908\text{ \AA}$, $c=12.32\text{ \AA}$, and $V=368.71(4)\text{ \AA}^3$.

The IR spectrometry technique sensitive to local structural distortions caused by defects provides information on the phase transitions that occur in $\text{Bi}_2(\text{Sn}_{0.95}\text{Cr}_{0.05})_2\text{O}_7$.

The IR spectroscopy investigations of 13-mm $\text{Bi}_2(\text{Sn}_{0.95}\text{Cr}_{0.05})_2\text{O}_7$ tablets in the KBr matrix were carried out on a VERTEX 80 v Fourier transform spectrometer with a spectral resolution of 1 cm^{-1} at temperatures of 110–525 K in the frequency range $350\text{--}1100\text{ cm}^{-1}$.

Permittivity investigations were conducted on an AM-3028 component analyzer in the temperature range 100–400 K at frequencies of up to 300 kHz.

3. Results and discussion

IR frequencies of the crystal lattice oscillations in $\text{Bi}_2(\text{Sn}_{0.95}\text{Cr}_{0.05})_2\text{O}_7$ are characteristic for the compounds with the pyrochlore structure and general chemical formula $\text{A}_2\text{B}_2\text{X}_7$. The absorption bands in IR spectra at frequencies of $100\text{--}1000\text{ cm}^{-1}$ correspond to oscillation of ions in the crystal lattice. These compounds have seven active stretching and bending IR modes [30,31], which are related to the oscillations of oxygen atoms occupying two crystallographic positions in the $\text{A}_2\text{B}_2\text{O}_6\text{O}'$ crystal structure. The unit cell of the crystal structure of bismuth pyrostannate $\text{Bi}_2\text{Sn}_2\text{O}_7$ is presented in Fig. 1.

Fig. 2 shows the absorption spectra of $\text{Bi}_2(\text{Sn}_{0.95}\text{Cr}_{0.05})_2\text{O}_7$ in the frequency range $350\text{--}1100\text{ cm}^{-1}$ at several temperatures. As the temperature is increased, the absorption line broadens. The similar temperature behavior of the IR spectra was observed for $\text{Bi}_{3/2}\text{MgNb}_{3/2}\text{O}_7$ and $\text{Bi}_{3/2}\text{Zn}_{0.92}\text{O}_{6.92}$ [31].

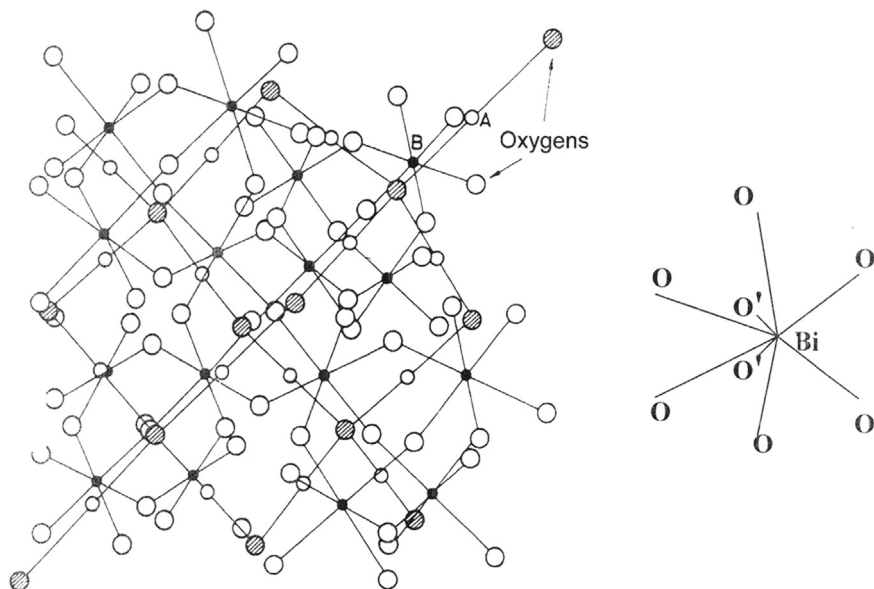


Fig. 1. Unit cell of the cubic pyrochlore structure $\text{Bi}_2\text{Sn}_2\text{O}_7$ with two interpenetrating networks of $\text{Bi}_2\text{O}'$ chains and SnO_6 octahedra. Symbols: A–Bi ions, B–Sn ions. Separately is shown the coordination environment around Bi atom in $\alpha\text{-Bi}_2\text{Sn}_2\text{O}_7$.

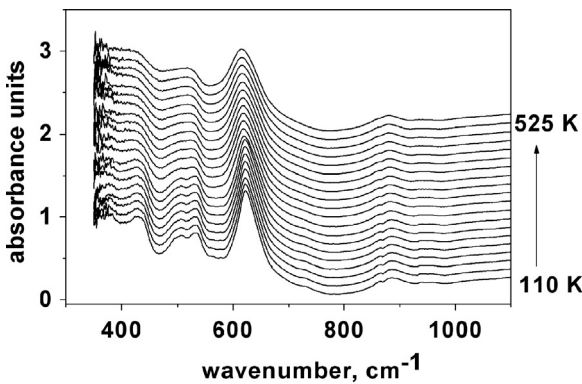


Fig. 2. Infrared spectra of the $\text{Bi}_2(\text{Sn}_{0.95}\text{Cr}_{0.05})_2\text{O}_7$ at several temperatures.

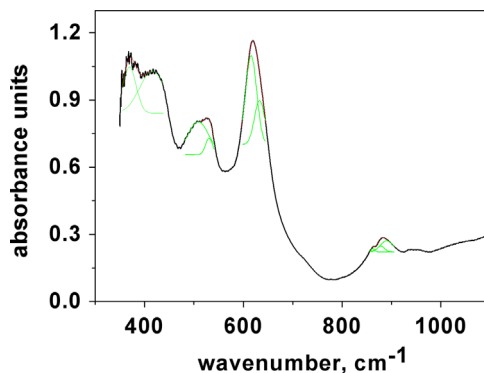


Fig. 3. Infrared spectra of the $\text{Bi}_2(\text{Sn}_{0.95}\text{Cr}_{0.05})_2\text{O}_7$ at room temperature.

The absorption line broadening can be associated with the structural or orientational disorder or anharmonicity of the oscillations. The orientational disorder was observed in titanium-bearing pyrochlore compounds and in bismuth oxide and its derivatives [32]. Random orientation of single A–O– Bi^{3+} and A–O’– Bi^{3+} electron pairs leads to the oscillation frequency spread and broadens the absorption spectrum [32].

Fig. 3 shows the room temperature IR spectrum of $\text{Bi}_2(\text{Sn}_{0.95}\text{Cr}_{0.05})_2\text{O}_7$, which involves four pronounced line groups in the frequency ranges 370–440, 480–560, 580–680, and 820–920 cm^{-1} . All the lines in the spectrum are complex and consist of several lines, specifically, two lines in the ranges 370–440, 480–560, and 580–680 cm^{-1} and three lines in the range 820–920 cm^{-1} . This is consistent with the coexistence of two polymorphic modifications in $\text{Bi}_2(\text{Sn}_{0.95}\text{Cr}_{0.05})_2\text{O}_7$, since the ion oscillation frequency is determined by the crystal lattice symmetry.

Two lines with frequencies of 378 and 416 cm^{-1} in the frequency range 370–440 cm^{-1} IR spectrum correspond to the oscillations of different ions in the lattice. According to the data reported in [31,33–35], the mode at a frequency of 382 cm^{-1} is the stretching Bi–O mode of the ideal pyrochlore structure. In our spectrum, this line is pronounced at low temperatures and blurred at higher ones, which can be caused by the sensitivity threshold of the measuring device. The line at 416 cm^{-1} corresponds to the oxygen oscillations in the SnO_6 octahedron.

The frequency range 490–540 cm^{-1} contains two broadened lines with frequencies of 506 and 526 cm^{-1} at room

temperature (Fig. 3). The mode at 506 cm^{-1} corresponds to the stretching oscillations of the Bi–O’ bond in the $\text{Bi}_2\text{Sn}_2\text{O}_7$ cubic phase [1] and the second line frequency (526 cm^{-1}) in our spectrum corresponds to the oscillations of the Bi–O’ bond in the orthorhombic phase.

In the frequency range 610–640 cm^{-1} , the room-temperature IR spectrum of $\text{Bi}_2(\text{Sn}_{0.95}\text{Cr}_{0.05})_2\text{O}_7$ consists of two lines with frequencies of 618 and 632 cm^{-1} (Fig. 3). Here, the IR absorption is attributed to the stretching oscillations of the Sn–O bond in the oxygen octahedron SnO_6 of the pyrochlore structure [31, 36–38] in both the cubic and orthorhombic phases.

In the high-frequency range (850–920 cm^{-1}), the absorption intensity is low. The absorption spectrum contains a shoulder at 863 cm^{-1} and a broadened line consisting of two lines at frequencies of 878 and 894 cm^{-1} . The similar mode was observed in several compounds with the pyrochlore structure, including $\text{Bi}_{3/2}\text{Zn}_{0.92}\text{Nb}_{1.5}\text{O}_{6.92}$ and $\text{Bi}_{3/2}\text{MgNb}_{3/2}\text{O}_7$ [31,39,40]. The IR spectra of these compounds contain very weak absorption lines at frequencies of 800–1100 cm^{-1} , which were determined as an additional complex structural mode related to the difference between ionic radii of metals. In the $\text{Bi}_2(\text{Sn}_{0.95}\text{Cr}_{0.05})_2\text{O}_7$ solid solution, substitution of chromium for tin leads to the local structure distortion in the vicinity of bismuth ions and the oscillations of the Bi–O’–Cr bonds correspond to these frequencies. As was mentioned in [41,42], the unshared Bi^{3+} electron pairs in some pyrochlores are shortened due to the overlap of Bi 6s electron pairs and d-orbitals of a B cation.

The Sn^{4+} , Cr^{3+} , and Bi^{3+} ionic radii are 0.067, 0.064, and 0.120 nm, respectively. Chromium ions occupy mainly the octahedral positions [43,44]. Therefore, we may assume that chromium replaces tin ions in SnO_6 and thus distorts the nearest environment. To ensure charge neutrality in the $\text{Bi}_2(\text{Sn}_{0.95}\text{Cr}_{0.05})_2\text{O}_7$, substitution of Cr^{3+} for Sn^{4+} possibly follows the scheme $3\text{Sn}^{4+} \rightarrow 4\text{Cr}^{3+}$. The similar scheme is implemented in the $\text{Bi}_2\text{O}_3\text{--ZnO}\text{--SnO}_2\text{--Nb}_2\text{O}_5$ system [38], in which Sn^{4+} , Zn^{2+} , and Nb^{5+} ions occupy B positions and the charge neutrality is ensured according the scheme $3\text{Sn}^{4+} \rightarrow \text{Zn}^{2+} + 2\text{Nb}^{5+}$.

The observed splitting of modes in the IR spectra of the $\text{Bi}_2(\text{Sn}_{0.95}\text{Cr}_{0.05})_2\text{O}_7$ (Fig. 3) is caused by the coexistence of phases with different lengths $L_{\text{C-A}}$ of the cation–anion bonds, which is confirmed within the mathematical pendulum model with the oscillation frequency $\omega^2 = L_{\text{C-A}} / M$, where M is the ion mass. The phases with different crystal symmetries have different electrostatic field gradients and force constants, K. The oscillation frequencies $\omega^2 = K/\mu$, where μ is the effective mass, will also be different.

The temperature dependence of phonon mode frequencies for $\text{Bi}_2(\text{Sn}_{0.95}\text{Cr}_{0.05})_2\text{O}_7$ is shown in Fig. 4. Almost all the oscillation frequencies monotonically decrease with increasing temperature, except for the frequency of oscillations of the Sn–O bond at 630 cm^{-1} (Fig. 4c). In the general case, the temperature dependence of frequency is written as

$$\Omega(T) = \omega_0 + \Delta\omega_{\text{lat}} + \Delta\omega_{\text{anh}} + \Delta\omega_{\text{el}}, \quad (1)$$

where ω_0 is the frequency of harmonic oscillations, $\Delta\omega_{\text{lat}}$ is the

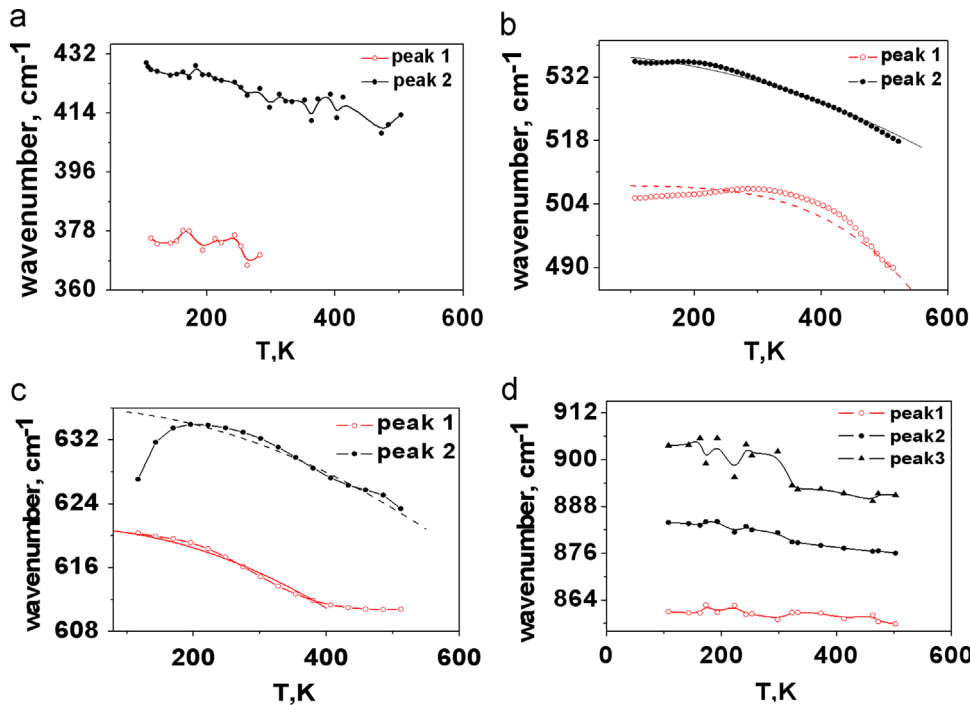


Fig. 4. The temperature dependence of the phonon frequencies of infrared spectra of the $\text{Bi}_2(\text{Sn}_{0.95}\text{Cr}_{0.05})_2\text{O}_7$. The solid and broken lines in (b) and (c) are fitting function of $\omega(T)=\omega_0+\Delta\omega_{\text{lat}}=\omega_0/\exp(B(T/T_c)^n)$.

frequency shift caused by the variation in the ion binding energy at the thermal expansion of the lattice and in the crystal structure under the action of strains or phase transitions, $\Delta\omega_{\text{anh}}$ is the frequency shift related to the anharmonicity of ion oscillations at the constant volume, and $\Delta\omega_{\text{el}}$ is the frequency shift at the electronic structure rearrangement as results of the electron-phonon interaction.

The anharmonic contribution to the temperature dependence of the oscillation frequency can be presented as inelastic collisions of two or three phonons with the same energy.

$$\Delta\omega_{i,\text{anh}}(T)=A(1+2/(e^x-1))+B(1+3/(e^y-1)+3/(e^y-1)^2), \quad (2)$$

where $x=E/2kT$, $y=E/3kT$, E is the phonon energy, and k is the Boltzmann constant. This contribution causes also the absorption line broadening: since coefficients A and B are positive, the frequency should increase upon sample heating.

We write the lattice contribution to the frequency in the form

$$\Delta\omega_{\text{qh}}^i(T)=\omega_{i0}\left\{\exp\left[-\int_0^T\gamma_i\alpha(T')dT'\right]-1\right\}, \quad (3)$$

where $\gamma_i=-\partial\ln\omega_i/\partial\ln V$ is the Gruneisen parameter of mode i and $\alpha(T)=1\partial V/V\partial T$ is the coefficient of thermal expansion. If γ and α are positive, the exponent is smaller than unity (<1) and this contribution is negative. Such a behavior is typical of positively expanding lattices. The Gruneisen parameter $\gamma_\alpha=-\partial\ln V\omega_\alpha/\partial\ln V=(B/\omega_\alpha)(\partial\omega_\alpha/\partial P)$ depends on the type of ion oscillation mode. The coefficients of thermal expansion will be different for different phases and, as a rule,

anomaly increase at the structural transition. Let us present the temperature dependence $\alpha(T)$ in the form of the power function in the region of structural transition: $\alpha(T)=\alpha_0(1+B(T/T_c)^n)$, where T_c is the transition temperature. The fitting function $\omega(T)=\omega_0+\Delta\omega_{\text{lat}}=\omega_0/\exp(B(T/T_c)^n)$ satisfactorily describes the experimental data with $B=0.042$, $T_c=430$ K, $n=2$, and $\omega_0=430$ cm⁻¹; $B=0.052$, $T_c=646$ K, $n=2$, and $\omega_0=536$ cm⁻¹; $B=0.048$, $T_c=548$ K, $n=4$, and $\omega_0=508$ cm⁻¹; $B=0.014$, $T_c=370$ K, $n=2$, and $\omega_0=620$ cm⁻¹; $B=0.024$, $T_c=548$ K, $n=2$, and $\omega_0=636$ cm⁻¹. The fitting parameter $B=\gamma\alpha_0\Delta T$ is consistent with the available estimates for oxides $\gamma=0.5-2$ [45], $\alpha_0=(2-5)\cdot10^{-5}$ K⁻¹, and $\Delta T=400$ K and the theoretical estimations yield the interval $B=0.01-0.04$.

Slight softening of frequencies of 878 and 894 cm⁻¹ upon heating is observed at a temperature of 330 K (Fig. 4d). At the same temperature, the absorption intensity sharply drops (Fig. 5d). This is possibly due to the electron contribution to the absorption spectrum. Impurity states of electrons (holes) form a bound state (polaron) with phonons. At a certain value of the electron-phonon interaction parameter, a quasi-gap is formed in the density of polaron impurity states. If the chemical potential lies within the lower polaron band, which is occupied incompletely, then electron transitions from the occupied state to the free ones occur with participation of phonons (e.g., at $T=150-160$ K). As a result, the absorption intensity sharply changes (Fig. 5a and c). As the temperature is increased, the chemical potential hits the forbidden polaron subband and the intensity of thermal transitions at $T=330$ K is decreased.

One more transition associated with the absorption intensity was observed near 260 K. The IR absorption attains its maximum value at a frequency of 508 cm⁻¹ (Fig. 5b) corresponding to the

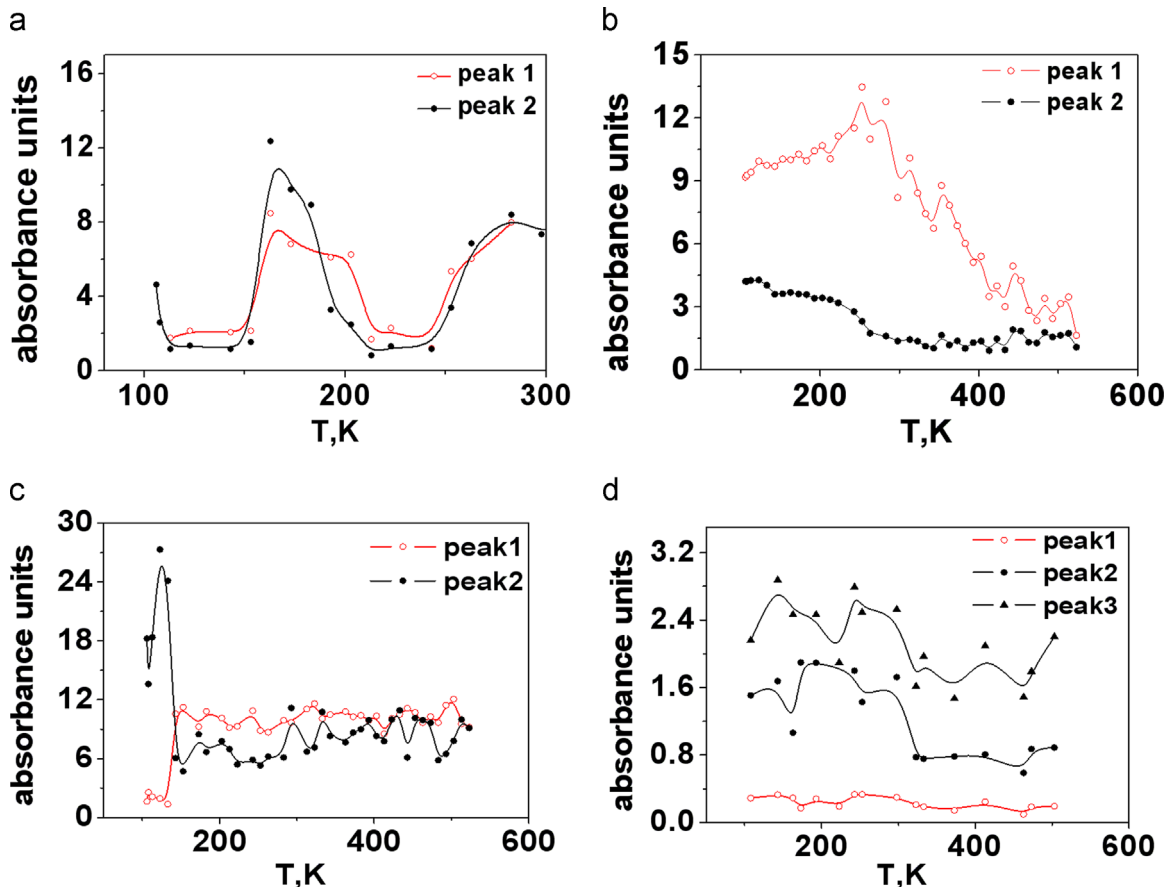


Fig. 5. The temperature dependence of the absorption intensity of phonon mode in the $\text{Bi}_2(\text{Sn}_{0.95}\text{Cr}_{0.05})_2\text{O}_7$.

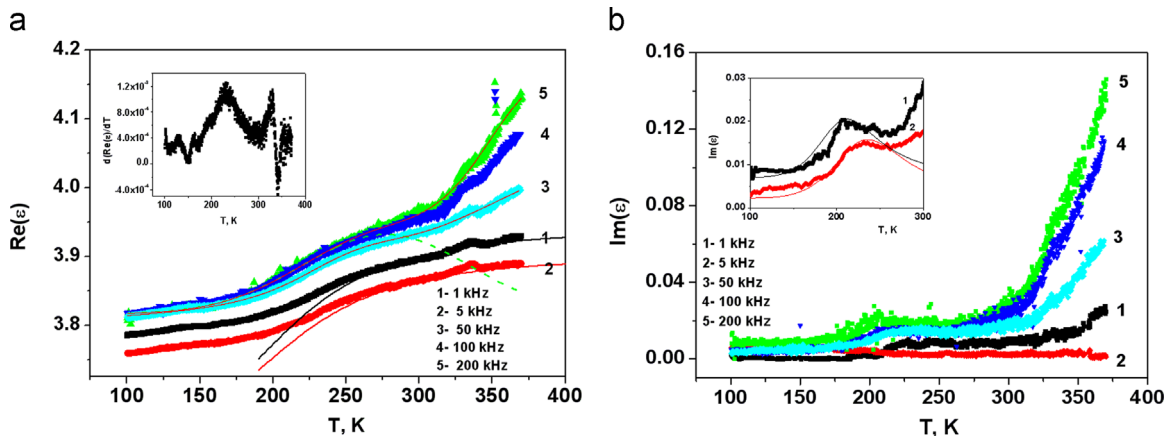


Fig. 6. The temperature dependence of the permittivity of the $\text{Bi}_2(\text{Sn}_{0.95}\text{Cr}_{0.05})_2\text{O}_7$. (a) Real part permittivity. The solid lines are fitting function in the Debye model $\text{Re}(\epsilon)=\text{Re}(\epsilon)(T=0)+A/(1+(B\omega \exp(\Delta E/kT)/T^2)^2)$. In the insert the curve $d(\text{Re}(\epsilon))/dT$ obtained at a frequency of 100 kHz. (b) Imaginary parts of the permittivity, the insert is the fitting function $\text{Im}(\epsilon)=\text{Im}(\epsilon)(T=0)+A\omega \exp(\Delta E/kT)/T^2/(1+(B\omega \exp(\Delta E/kT)/T^2)^2)$.

oscillations of the single $\text{Bi}-\text{O}'$ bond. Possibly, the symmetry center is formed in one of the phases; i.e., the phase transition centrosymmetrical–noncentrosymmetrical structure occurs. This assumption is confirmed by the permittivity maximum at 260 K (Fig. 6).

Fig. 6 shows the temperature dependence of the real and imaginary parts of permittivity. We can distinguish three intervals in the dependence $\epsilon(T)$. Upon heating to 200 K, the real part of permittivity of the $\text{Bi}_2(\text{Sn}_{0.95}\text{Cr}_{0.05})_2\text{O}_7$ increases; the temperature dependence of $\text{Re}(\epsilon)$ has an inflection point

above 200 K, which depends on frequency. The curve $d(\text{Re}(\epsilon))/dT$ obtained at a frequency of 100 kHz contains a peak near $T=230$ K (insert to Fig. 6a). Above 300 K, the dependence $\epsilon(T)$ is determined by frequency; at $\omega > 50$ kHz, the permittivity sharply increases at 50 kHz and attains its maximum at the temperature of the transition $\alpha \rightarrow \beta$. The permittivity growth is caused by conduction electrons. In the $\text{Bi}_2\text{Sn}_2\text{O}_7$ compound [25], the conductivity has a small peak at $T=250$ K, which is related to electron hoppings between the impurity states. Above 250 K, the growth of $\text{Re}(\epsilon)$ becomes

slower below 50 kHz due to diffusion of defects over the lattice. The defect relaxation time is $\tau = \lambda^2/2D$, where λ is the average path length of an oxygen ion over the defects and D is the coefficient ion diffusivity. The temperature dependence of the diffusivity has the activation character: $D = D_0 \exp(-\Delta E/kT)$, where ΔE is the energy barrier. During diffusion, local lattice strains occur, which induce acoustic phonon excitations; therefore, $\lambda \sim 1/N \sim 1/T$, where N is the number of phonons. The fitting function in the Debye model has the form

$$\begin{aligned} \text{Re}(\epsilon) &= \text{Re}(\epsilon)(T=0) + A/(1+(\omega\tau)^2) \\ &= \text{Re}(\epsilon)(T=0) + A/(1+(B\omega \exp(\Delta E/kT)/T^2)^2), \end{aligned} \quad (4)$$

and satisfactorily describes the experimental data above 250 K with fitting parameters A and B and $\Delta E = 0.1$ eV (Fig. 6a).

The temperature dependence $\text{Re}(\epsilon)$ for the frequencies $\omega > 50$ kHz can be presented in the form of two maxima with the Gaussian function (Fig. 6a). The temperature of the transition in the high-temperature region is frequency-independent and at low temperatures logarithmically shifts toward lower temperatures with increasing frequency from $T^* = 268$ K at $\omega = 50$ kHz to $T^* = 260$ K at $\omega = 200$ kHz. This can be attributed to electron tunneling between the polar Bi–O' bonds in the unit cell.

The maximum of the imaginary part of permittivity shifts to the high-temperature region from $T^* = 207$ K at $\omega = 50$ kHz to $T^* = 230$ K at $\omega = 200$ kHz. This is explained using the Debye model for susceptibility

$$\text{Im } \chi = \chi_0(\omega\tau)/(1+(\omega\tau)^2), \quad (5)$$

where $\tau = \tau_0 \exp(\Delta E/kT)/T^2$, χ_0 is the static dielectric susceptibility, and τ_0 is the frequency factor. The fitting function

$$\begin{aligned} \text{Im}(\epsilon) &= \text{Im}(\epsilon)(T=0) + A(\omega\tau)/(1+(\omega\tau)^2) \\ &= \text{Im}(\epsilon)(T=0) + A\omega \exp(\Delta E/kT)/T^2 / \\ &\quad (1+(B\omega \exp(\Delta E/kT)/T^2)^2) \end{aligned}$$

describes well the experimental data and the shift of the maximum with an increase the frequency using the fitting parameters A and B and $\Delta E = 0.1$ eV (Fig. 5b). Comparison of the model calculations with the experiment indicates a decrease in the ion free path length with increasing frequency of the external electric field.

The intensity maxima in the IR absorption spectrum in the frequency ranges 370–440 and 480–560 cm⁻¹ (Fig. 5) near 150 K are consistent with the magnetic measurement data for $\text{Bi}_2(\text{Sn}_{0.95}\text{Cr}_{0.05})_2\text{O}_7$. At the same temperature, the magnetic susceptibility of $\text{Bi}_2(\text{Sn}_{0.95}\text{Cr}_{0.05})_2\text{O}_7$ changes its sign (Fig. 7). The field dependence of magnetization indicated the trivalent state of chromium ions [28] with the spin $S = 3/2$. The magnetic susceptibility contains the paramagnetic term χ_p of chromium ion spins and diamagnetic term χ_d of bismuth and tin ions

$$\chi^{th} = C/(T-\theta) + \chi_p \quad (6)$$

This function describes well the experimental susceptibility data with the parameters $C = 1.9$, $\theta = 2$ K, and $\chi_p = -0.015$ emu/g. In the temperature range 110–160 K, the experimental data

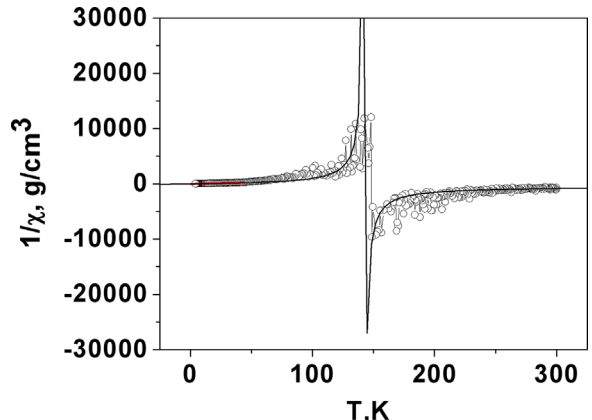


Fig. 7. The temperature dependence of the inverse magnetic susceptibility of the $\text{Bi}_2(\text{Sn}_{0.95}\text{Cr}_{0.05})_2\text{O}_7$. The solid line is function $\chi^{th} = C/(T-\theta) + \chi_p$.

on $\chi^{ex}(T)$ exceed the values of $\chi^{th}(T)$ calculated using formula (6). The occurrence of the additional paramagnetic contribution is caused by impurity electrons at the chemical potential level.

4. Conclusions

It was established that the IR spectra of the bismuth pyrostannate ($\text{Bi}_2(\text{Sn}_{0.95}\text{Cr}_{0.05})_2\text{O}_7$) contain four frequency ranges with two absorption lines in each of them and three absorption lines in the high-frequency range, which correspond to the two-phase state. Softening of frequencies was observed and the type of oscillation mode related to the bismuth and tin valence bonds at the structural transitions was determined. It was found that the magnetic susceptibility changes its sign at low temperatures and the temperature dependence of permittivity has the maximum near 260 K, which agrees well with the temperatures of maximum IR absorption line intensity. The temperature shifts of the oscillation frequencies were described through the variation in the binding energy of ions at the phase transitions with the use of the coefficient of thermal expansion. The experimental results were explained within the model of polaron impurity states and diffusion of oxygen ions over lattice defects in the Debye model.

Acknowledgment

This work was supported by the Russian Foundation for Basic Research Projects no. 15-42-04099 r_siberia_a, Siberian Branch of Science and NAS of Belarus "Electronic and magnetic phase transitions in materials with magnetoelectric affect" and government work no. 114090470016.

References

- [1] R.X. Silva, C.W.A. Paschoal, R.M. Almedia, M. Carvalho Castro Jr., A. P. Ayala, Jeffrey T. Auletta, Michael W. Lufaso, Temperature dependence Raman spectra of $\text{Bi}_2\text{Sn}_2\text{O}_7$, Vib. Spectrosc. 64 (2013) 172–177.
- [2] T. Fennell, O.A. Petrenko, B. Fak, S.T. Bramwell, M. Enjalran, T. Yavors'kii, M.J.P. Gingras, R.G. Melko, G. Balakrishnan, Neutron scattering investigation of the spin ice state in $\text{Dy}_2\text{Ti}_2\text{O}_7$, Phys. Rev. B 70 (2004) 134408.
- [3] A.P. Ramirez, A. Hayashi, R.J. Cava, R. Siddharthan, B.S. Shastry, Zero point entropy in spin ice, Nature. 399 (1999) 333–335.

- [4] S.T. Bramwell, M.J. Harris, B.C. den Hertog, M.J.P. Gingras, J. S. Gardner, D.F. McMorrow, A.R. Wildes, A.L. Cornelius, J.D. M. Champion, R.G. Melko, T. Fennell., Spin correlations in $\text{Ho}_2\text{Ti}_2\text{O}_7$: a dipolar spin ice system, *Phys. Rev. Lett.* 87 (2001) 047205.
- [5] J.S. Gardner, B.D. Gaulin, A.J. Berlinsky, P. Waldron, S.R. Dunsiger, N. P. Raju, J.E. Greedan, Neutron scattering studies of the cooperative paramagnet pyrochlore $\text{Tb}_2\text{Ti}_2\text{O}_7$, *Phys. Rev. B* 64 (2001) 224416.
- [6] S.W. Han, J.S. Gardner, C.H. Booth, Structural properties of the geometrically frustrated pyrochlore $\text{Tb}_2\text{Ti}_2\text{O}_7$, *Phys. Rev. B* 69 (2004) 24416.
- [7] J.D.M. Champion, M.J. Harris, P.C.W. Holdsworth, W.S. Wills, G. Balakrishnan, S.T. Bramwell, E. Čížmár, T. Fennell, J.S. Gardner, J. Lago, D.F. McMorrow, M. Orendáč, A. Orendáčová, D. McK Paul, R. I. Smith, M.T.F. Telling, A. Wildes, $\text{Er}_2\text{Ti}_2\text{O}_7$: evidence of quantum order by disorder in a frustrated antiferromagnet, *Phys. Rev. B* 68 (2003) 20401 (R).
- [8] J.D.M. Champion, A.S. Wills, T. Fennell, S.T. Bramwell, J.S. Gardner, M.A. Green, Order in the Heisenberg pyrochlore: the magnetic structure of $\text{Gd}_2\text{Ti}_2\text{O}_7$, *Phys. Rev. B* 64 (2001) 140407 (R).
- [9] N.P. Raju, M. Dion, M.J.P. Gingras, T.E. Mason, J.E. Greedan, Transition to long-range magnetic order in the highly frustrated insulating pyrochlore antiferromagnet $\text{Gd}_2\text{Ti}_2\text{O}_7$, *Phys. Rev. B* 59 (1999) 14489.
- [10] R. Jin, J. He, S. McCall, C.S. Alexander, F. Drymiotis, D. Mandrus., Superconductivity in the correlated pyrochlore $\text{Cd}_2\text{Re}_2\text{O}_7$, *Phys. Rev. B* 64 (2001) 180503 (R).
- [11] S.A. Kramer, H.L. Tuller, A novel titanate-based oxygen ion conductor: $\text{Gd}_2\text{Ti}_2\text{O}_7$, *Solid State Ion.* 82 (1995) 15.
- [12] C. Heremans, B.J. Wuensch, J.K. Stalick, E.J. Prince, Fast-ion conducting $\text{Y}_2(\text{Zr}_{1-y})_2\text{O}_7$ pyrochlores: neutron rietveld analysis of disorder induced by Zr substitution, *Solid State Chem.* 117 (1995) 108.
- [13] C.A. Mims, A.J. Jacobson, R.B. Hall, J.T. Lewandowski, Methane oxidative coupling over nonstoichiometric bismuth–tin pyrochlore catalysts, *J. Catal.* 153 (1995) 197.
- [14] L. Moens, P. Ruiz, B. Delmon, M. Devillers, Cooperation effects towards partial oxidation of isobutene in multiphasic catalysts based on bismuth pyrostannate, *Appl. Catal. A: Gen.* 171 (1998) 131.
- [15] L. Moens, P. Ruiz, B. Delmon, M. Devillers, Evaluation of the role played by bismuth molybdates in $\text{Bi}_2\text{Sn}_2\text{O}_7\text{-MoO}_3$ catalysts used for partial oxidation of isobutene to methacrolein, *Appl. Catal. A Gen.* 180 (1999) 299.
- [16] L. Moens, P. Ruiz, B. Delmon, M. Devillers, A simplified partial ionic charge model to evaluate the role played by bismuth pyrostannate in multiphase catalysts for the selective oxidation of isobutene to methacrolein, *Appl. Catal. A Gen.* 180 (1999) 299.
- [17] G.S. Devi, S.V. Manorama, V.I. Rao, $\text{SnO}_2/\text{Bi}_2\text{O}_3$: a suitable system for selective carbon monoxide detection, *J. Electrochem. Soc.* 145 (1998) 1039.
- [18] G.S. Devi, S.V. Manorama, V.I. Rao, $\text{SnO}_2\text{-Bi}_2\text{O}_3$ based CO sensor: laser-Raman, temperature programmed desorption and X-ray photoelectron spectroscopic studies, *Sens. Actuators B: Chem.* 56 (1999) 98.
- [19] T.D. Malinovskaya, A.I. Aparnev, Y.P. Egorov, Y.M. Yukhin, Carbon monoxide semiconductor sensors based on $\text{SnO}_2\text{-Bi}_2\text{O}_3$, *Russ. J. Appl. Chem.* 74 (2001) 1864.
- [20] R.D. Shannon, J.D. Bierlein, J.L. Gillson, G.A. Jones, A.W. Sleight, Polymorphism in $\text{Bi}_2\text{Sn}_2\text{O}_7$, *J. Phys. Chem. Solids* 41 (1980) 117.
- [21] V. Kahlenberg, Th Zeiske, Structure of $\gamma\text{-Bi}_2\text{Sn}_2\text{O}_7$ by high temperature powder neutron diffraction, *Z. Krist.* 212 (1997) 297–301.
- [22] I.R. Evans, J.A.K. Howard, J.S.O. Evans, $\alpha\text{-Bi}_2\text{Sn}_2\text{O}_7$ – a 176 atom crystal structure from powder diffraction data, *J. Mater. Chem.* 13 (2003) 2098–2103.
- [23] B.J. Kennedy, I.M. Elcombe, Structure and Bonding in $\text{Bi}_2\text{Sn}_2\text{O}_7$, *Mater. Sci. Forum* 278 (1998) 762–767.
- [24] A. Salamat, A.L. Hector, P.F. McMillan, C. Ritter, Structure, bonding, and phase relations in $\text{Bi}_2\text{Sn}_2\text{O}_7$ and $\text{Bi}_2\text{Ti}_2\text{O}_7$ pyrochlores: new insights from high pressure and high temperature studies, *Inorg. Chem.* 50 (2011) 11905–11913.
- [25] L.V. Udod, S.S. Aplesnin, M.N. Sitnikov, M.S. Molokeev, Dielectric and electrical properties of polymorphic bismuth pyrostannate $\text{Bi}_2\text{Sn}_2\text{O}_7$, *Phys. Solid State* 56 (2014) 1315–1319.
- [26] G.A. Petrakovskii, K.A. Sablina, L.V. Udod, A.I. Pankrats, D. A. Velikanov, R. Szymczak, M. Baran, G.V. Bondarenko, Effect of Ni-substitution on magnetic phase transition in CuB_2O_4 , *J. Magn. Magn. Mater.* 300 (2006) e476–e478.
- [27] G.A. Petrakovskii, L.V. Udod, K.A. Sablina, A.I. Pankrats, S. N. Martynov, D.A. Velikanov, R. Szymczak, M. Baran, A.F. Bovina, G.V. Bondarenko, Effect of substitution on the magnetic properties of CuB_2O_4 , *Phys. Metals Metallogr.* 99 (Suppl. 1) (2005) S53–S56.
- [28] S.S. Aplesnin, L.V. Udod, M.N. Sitnikov, E.V. Eremin, M.S. Molokeev, L.S. Tarasova, K.I. Yanushkevich, A.I. Galyas, Correlation of magnetic and transport properties with polymorphic transitions in bismuth pyrostannate $\text{Bi}_2(\text{Sn}_{1-x}\text{Cr}_x)_2\text{O}_7$, *Phys. Solid State* 57 (2015) 1590–1595.
- [29] L.V. Udod, M.N. Sitnikov, S.S. Aplesnin, M.S. Molokeev, Electrical and dielectrical properties of gas-sensor resistive type $\text{Bi}_2\text{Sn}_2\text{O}_7$, *Solid State Phenom.* 215 (2014) 503–506.
- [30] M.A. Subramanian, G. Aravamudan, G.V. Subba Rao, Oxide pyrochlores-a review, *Prog. Solid State Chem.* 15 (1983) 55–143.
- [31] M. Chen, D.B. Tanner, J.C. Nino, Infrared study of the phonon modes in bismuth pyrochlores, *Phys. Rev. B* 72 (2005) 054303–054308.
- [32] R.J. Betsch, W.B. White, Vibrational spectra of bismuth oxide and the sillenite-structure bismuth oxide derivatives, *Spectrochim. Acta Part A* 34 (1978) 505–514.
- [33] H. Wang, A. Serquis, B. Maiorov, L. Civale, Q.X. Jia, P.N. Arendt, S. R. Foltyn, J.L. MacManus-Driscoll, X. Zhang, Microstructure and transport properties of Y-rich $\text{YBa}_2\text{Cu}_3\text{O}_{7-\delta}$ thin films, *J. Appl. Phys.* 100 (2006) 053904-4.
- [34] M. Fischer, T. Malcherek, U. Bismayer, P. Blaha, K. Schwarz, Structure and stability of $\text{Cd}_2\text{Nb}_2\text{O}_7$ and $\text{Cd}_2\text{Ta}_2\text{O}_7$ explored by ab initio calculations, *Phys. Rev. B* 78 (2008) 014108–014108.
- [35] T.A. Vanderah, I. Levin, M.W. Lufaso, An unexpected crystal-chemical principle for the pyrochlore structure, *Eur. J. Inorg. Chem.* 14 (2005) 2895–2905.
- [36] S. Brown, H.C. Gupta, J.A. Alonso, M.J. Martínez-Lope, Lattice dynamical study of optical modes in $\text{Tl}_2\text{Mn}_2\text{O}_7$ and $\text{In}_2\text{Mn}_2\text{O}_7$ pyrochlores, *Phys. Rev. B* 69 (2004) 054434–054436.
- [37] M. Maćzka, M.L. Sanjuán, A.F. Fuentes, K. Hermanowicz, J. Hanuza, Temperature-dependent Raman study of the spin-liquid pyrochlore $\text{Tb}_2\text{Ti}_2\text{O}_7$, *Phys. Rev. B* 78 (2008) 134420–134428.
- [38] H. Du, X. Yao, L. Zhang, Structure, IR spectra and dielectric properties of $\text{Bi}_2\text{O}_3\text{-ZnO-SnO}_2\text{-Nb}_2\text{O}_5$ quaternary pyrochlore, *Ceram. Int.* 28 (2002) 231–234.
- [39] R.L. Withers, T.R. Welberry, A.-K. Larsson, Y. Liu, L. Norén, H. Rundlöf, F.J. Brink, Local crystal chemistry, induced strain and short range order in the cubic pyrochlore $(\text{Bi}_{1.5-\alpha}\text{Zn}_{0.5-\beta})(\text{Zn}_{0.5-\gamma}\text{Nb}_{1.5-\delta})\text{O}_{(7-1.5\alpha-\beta-\gamma-2.5\delta)}$ (BZN), *J. Solid State Chem.* 177 (2004) 231–244.
- [40] R.A. McCauley, Infrared-absorption characteristics of the pyrochlore structure, *J. Opt. Soc. Am.* 63 (1973) 721–725.
- [41] R.D. Shannon, Revised effective ionic radii and systematic studies of interatomic distances in halides and chalcogenides, *Acta Cryst. A* 32 (1976) 751–767.
- [42] B.J. Kennedy, Structural trends in Bi containing pyrochlores: The structure of $\text{Bi}_2\text{Rh}_2\text{O}_{7-\delta}$, *Mater. Res. Bull.* 32 (1997) 479–483.
- [43] I. Jendrzejewska, J. Mroziński, P. Zajdel, T. Mydlarz, T. Goryczka, A. Hanc, E. Maciążek, X-Ray and magnetic investigations of the polycrystalline compounds with general formula $\text{Zn}_x\text{Sn}_y\text{Cr}_z\text{Se}_4$, *Arch. Metall. Mater.* 54 (2009) 723–730.
- [44] A.A. Pandit, S.S. More, R.G. Dorik, K.M. Jadhav, Structural and magnetic properties of $\text{Co}_{1+y}\text{Sn}_y\text{Fe}_{2-2y-x}\text{Cr}_x\text{O}_4$ ferrite system, *Bull. Mater. Sci.* 26 (2003) 517–521.
- [45] A.B. Medvedev, R.F. Trunin, Shock compression of porous metals and silicates, *Phys. Uspekhi* 55 (2012) 829–846.